Received: 26 March 2019 | Revised: 13 May 2019 | Accepted: 16 May 2019

DOI: 10.1002/dvdy.63

RESEARCH ARTICLE

Developmental Dynamics WILEY

Sub-micrometer insights into the cytoskeletal dynamics and ultrastructural diversity of butterfly wing scales

Christopher R. Day[1,2] | **Joseph J. Hanly**[1] | **Anna Ren**[1] | **Arnaud Martin**[1]

[1]Department of Biological Sciences, The George Washington University, Washington, District of Columbia

[2]Epigenetics and Stem Cell Biology Laboratory, National Institute of Environmental Health Sciences, National Institutes of Health, Durham, North Carolina

Correspondence
Arnaud Martin, Department of Biological Sciences, 800 22nd Street NW, SEH #6000, Washington, DC 20052
Email: arnaud@gwu.edu

Funding information
National Science Foundation, Grant/Award Numbers: IOS-1755329, IOS-1656553

ABSTRACT

Background: The color patterns that adorn lepidopteran wings are ideal for studying cell type diversity using a phenomics approach. Color patterns are made of chitinous scales that are each the product of a single precursor cell, offering a 2D system where phenotypic diversity can be studied cell by cell, both within and between species. Those scales reveal complex ultrastructures in the sub-micrometer range that are often connected to a photonic function, including iridescent blues and greens, highly reflective whites, or light-trapping blacks.

Results: We found that during scale development, Fascin immunostainings reveal punctate distributions consistent with a role in the control of actin patterning. We quantified the cytoskeleton regularity as well as its relationship to chitin deposition sites, and confirmed a role in the patterning of the ultrastructures of the adults scales. Then, in an attempt to characterize the range and variation in lepidopteran scale ultrastructures, we devised a high-throughput method to quickly derive multiple morphological measurements from fluorescence images and scanning electron micrographs. We imaged a multicolor eyespot element from the butterfly *Vanessa cardui* (*V. cardui*), taking approximately 200 000 individual measurements from 1161 scales. Principal component analyses revealed that scale structural features cluster by color type, and detected the divergence of non-reflective scales characterized by tighter cross-rib distances and increased orderedness.

Conclusion: We developed descriptive methods that advance the potential of butterfly wing scales as a model system for studying how a single cell type can differentiate into a multifaceted spectrum of complex morphologies. Our data suggest that specific color scales undergo a tight regulation of their ultrastructures, and that this involves cytoskeletal dynamics during scale growth.

KEYWORDS
chitin, cytoskeleton, F-actin, fascin, insect scales, nano-morphometrics, ultrastructures

1 | INTRODUCTION

The study of cell type diversity has historically relied on high-throughput molecular profiles of the genome, transcriptome, proteome, and metabolome, rather than by characterization of cell morphology or physiology. While cell phenotypes inform us about structure-function relationships and remain an important output of diversity,[1,2] to our knowledge, only yeast cells have been subject to a multi-dimensional profiling of their physical characteristics, or "phenomics".[3,4] Thus, new model

Christopher Day and Joseph Hanly have contributed equally to this work and share first authorship.

systems are needed to tackle how cellular morphologies are generated and modulated in multicellular organisms.

The simplicity and diversity of butterfly wings, consisting of a flat canvas of nondividing cells that each yield a single color, in the manner of pixels on a screen, provides a rare opportunity to investigate these questions. Butterfly wings consist of 2D arrays of color units that display tremendous diversity, both within a wing pattern and between species.[5] Wing patterns are made of hundreds of thousands of scales that derive their color from pigments, ultrastructure, or a combination of the two.[6,7] Scale structures interact with light through a variety of mechanisms that have been described from a biophysical perspective,[8] including light-trapping black,[9-11] light polarization,[12] high-reflectance,[13] transparency,[14] and color-selective iridescence.[15-19] For instance, the coherent light-scattering features of *Morpho* butterflies reflect specific wavelengths, producing their characteristic blue iridescence.[20] In this butterfly, ridge stacking (the dense piling of multiple layers of lamellae) combined with short inter-ridge distances scatters long wavelengths of light while reflecting wavelengths in the blue range.[21-23] Some pierid butterflies have convergently evolved ridge density and stacking that produce iridescence, albeit in the ultraviolet range.[24] In contrast, the green iridescence of certain lycaenid butterflies is produced by gyroid-shaped photonic crystals derived from cell endomembranes.[25] Beyond the remarkably diverse optical properties of these sub-micrometer features, it is also worth mentioning that pheromone scales specialized in the emission or retention of volatile compounds also display a biodiverse array of ultrastructures.[26,27] Thus, lepidopteran wings offer a rich morphospace of structure-function relationships that are awaiting a systematic cell-by-cell characterization.

To date, our understanding of the ontogenesis of lepidopteran wing scale ultrastructures is scarce. Each chitinous scale emerges from a single cell during pupal development of the wing.[28,29] Beginning at approximately 20% of development, bundles of actin filaments start extruding a growing scale extension through a socket cell.[30,31] By 40% of pupal development, the actin bundles have organized into a highly ordered pattern and direct the deposition of chitin into parallel structures.[14] The resulting scale consists of highly ordered ridges of lamellae connected by crossribs. These crossribs are supported by rods called trabeculae, that interact with the lower lamina and provide scaffolding support to the scale structure.[32,33] The crossribs often leave unfilled windows that reveal the inner architecture of the scale; in other cases, deposition of ectopic lamina can close the windows formed by ridges and crossribs, changing the reflective properties of the scale. Scanning electron microscopy (SEM) has been used to survey the variation in scale structure within and between species in a variety of butterflies. Early descriptions of scale structure in *Heliconius* described three distinct scale types, which are coupled to color.[34] In *Bicyclus*, the coupling of color and structure shows a more continuous variation[35] and, of interest, CRISPR mutagenesis of melanin synthesis pathway genes in this butterfly affect scale morphology.[36] Thus, in addition to the importance of cytoskeletal dynamics and chitin deposition, melanin content, or the recruitment of that pathway during scale maturation may also influence scale morphology by fine-tuning cuticle sclerotization.[37,38]

Being able to measure a large number of variables at once, across large fields of scales, would be a first step for characterizing scale diversity cell by cell, both within and between species. Qualitative and quantitative studies of scale ultrastructures have usually focused on a small number of scales using manual measurements taken from electron micrographs, but we are now starting to see new methods that can increase either resolution or sample size. Scanning probe microscopy (SPM) is unique in its ability to provide topographical data (eg, ridge height), but is limited to single scales.[16,39,40] In contrast, small angle X-ray scattering (SAXS) has been used across larger regions, and yielded precise measurements of gyroid crystals and ridge spacing[16,41,42]; while this technique can be implemented on hundreds of wing samples, it requires access to a beamline, does not allow the extraction of multiple variables, and is more suited to homogenous wing surfaces rather than to complex, multicolor patterns.

Here, we devise new methods for the study of scale ultrastructural differentiation and diversification, using the wing scales of the Painted Lady butterfly, *V. cardui* (Figure 1). Following-up on previous research,[30] we strengthen the evidence that F-actin bundles set-up ridge spacing, and identify Fascin as a possible mediator of cytoskeletal modulations. Then, we describe a semi-automated method to quickly extract a variety of morphometric measurements from fluorescence images and 2D SEM images. Deploying a comprehensive analysis of cover scales across an entire pattern element, we identify subtle correlations between ultrastructural variation and color types. Overall, this work enables future studies that aim to decipher the generation of morphological diversity across fields of insect integumentary cells.

2 | RESULTS

2.1 | Actin dynamics prepattern the Vanessa cardui scale ridge spacing

As previously reported,[30] confocal imaging of 40% developed pupae revealed evenly interspersed F-actin bundles and chitin deposition ridges running along the length of the scale (Figure 2A). 3D reconstruction of confocal z-stacks, as well as fluorescence intensity profiles, confirmed that chitin deposition along the presumptive ridges occurs between and slightly above F-actin bundles (Figure 2B,C). To further investigate the relationship between F-actin bundles and deposited chitin

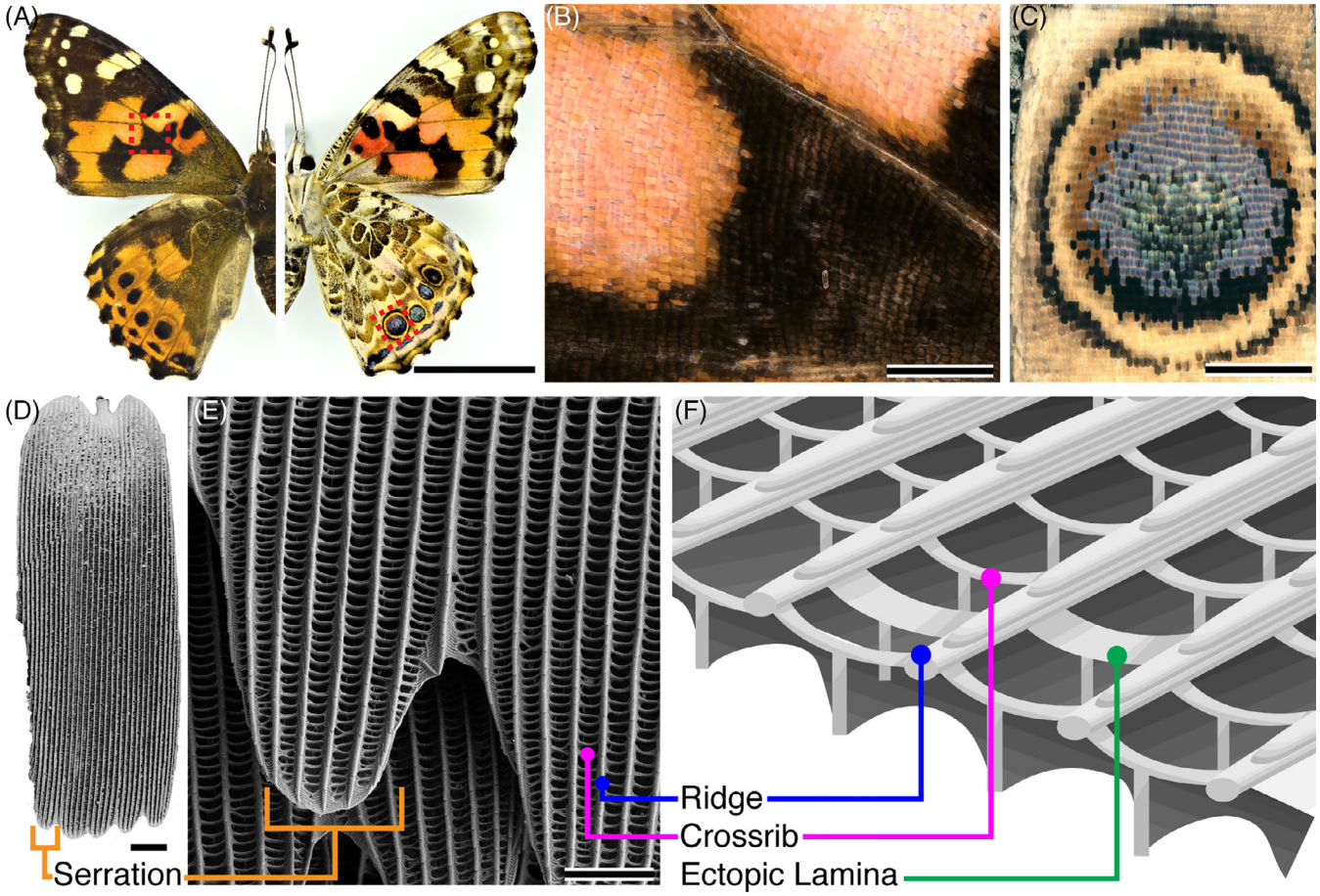

FIGURE 1 Pattern elements and scale ultrastructural features in *V. cardui*. A, Dorsal (left) and ventral (right) surfaces of *V. cardui* wings. Red dashed boxes: areas of interest magnified in panels B,C. Scale bar = 1 cm. B, Magnified view of the black/orange pattern from the dorsal forewing. C, Magnified view of the of the Cu1-Cu2 ventral eyespot. D,E, SEM micrographs of a single *V. cardui* wing scale. F, Schematic view of a scale cross-section, with the upper surface showing ridges, crossribs, and ectopic lamina are represented. The lower surface of *V. cardui* wings shows a monolayered basal lamina not represented here.[17,18] Scale bars = 1 cm in A; 1 mm in B,C; 10 μm in D; 5 μm in E

ridges, the fluorescence intensity profile traces were Fourier-transformed and the modal spacing extracted. There was no statistical difference in spacing between the chitin ridges and actin bundles (Wilcoxon signed-rank test, $P > 0.58$), highlighting a tight coupling between the cytoskeletal patterning and the localization of ridge building at this developmental stage (Figure 2D). Then we compared the features of late pupal wings (~95% development, after scale pigmentation had begun, Figure 2E) and adult scales from the corresponding region of the wing (Figures 1C and 2G). Scales before adult emergence showed higher ridge spacing than in the adult sample (1.76 ± 0.20 μm and 1.61 ± 0.24 μm, respectively); *t*-test, $P < 0.002$). It is unlikely that this ~9.3% difference derives from inter-individual variation, indicating there could be turgor pressure in the late pupal scales causing a small amount of expansion, or that the scale exoskeleton contracts as it dries after imago emergence.

In addition, we also found that a mouse monoclonal antibody targeting Singed, the *Drosophila* homolog of vertebrate Fascin,[43] cross-hybridizes in butterflies and shows localized punctate signals in the developing scale around 40% of development (Figure 3). This immunolocalization resembles the one observed in *Drosophila* developing bristles, and is consistent with the known role of Fascin in the patterning and branching of F-actin bundles.[44] Thus, Fascin may play a role in modulating ridge spacing, and we speculate that its density or activity may vary in butterflies with radically different ultrastructures.

2.2 | High-throughput phenomics on an entire color pattern element

Our developmental data confirm a role of cytoskeletal and chitin-deposition dynamics in the making of complex ultrastructures, and is presently suited to simple comparisons between a small number of scale types. Further work and technological development is needed to speed up image acquisition and allow cytoskeletal resolutions over large and heterogenous fields of

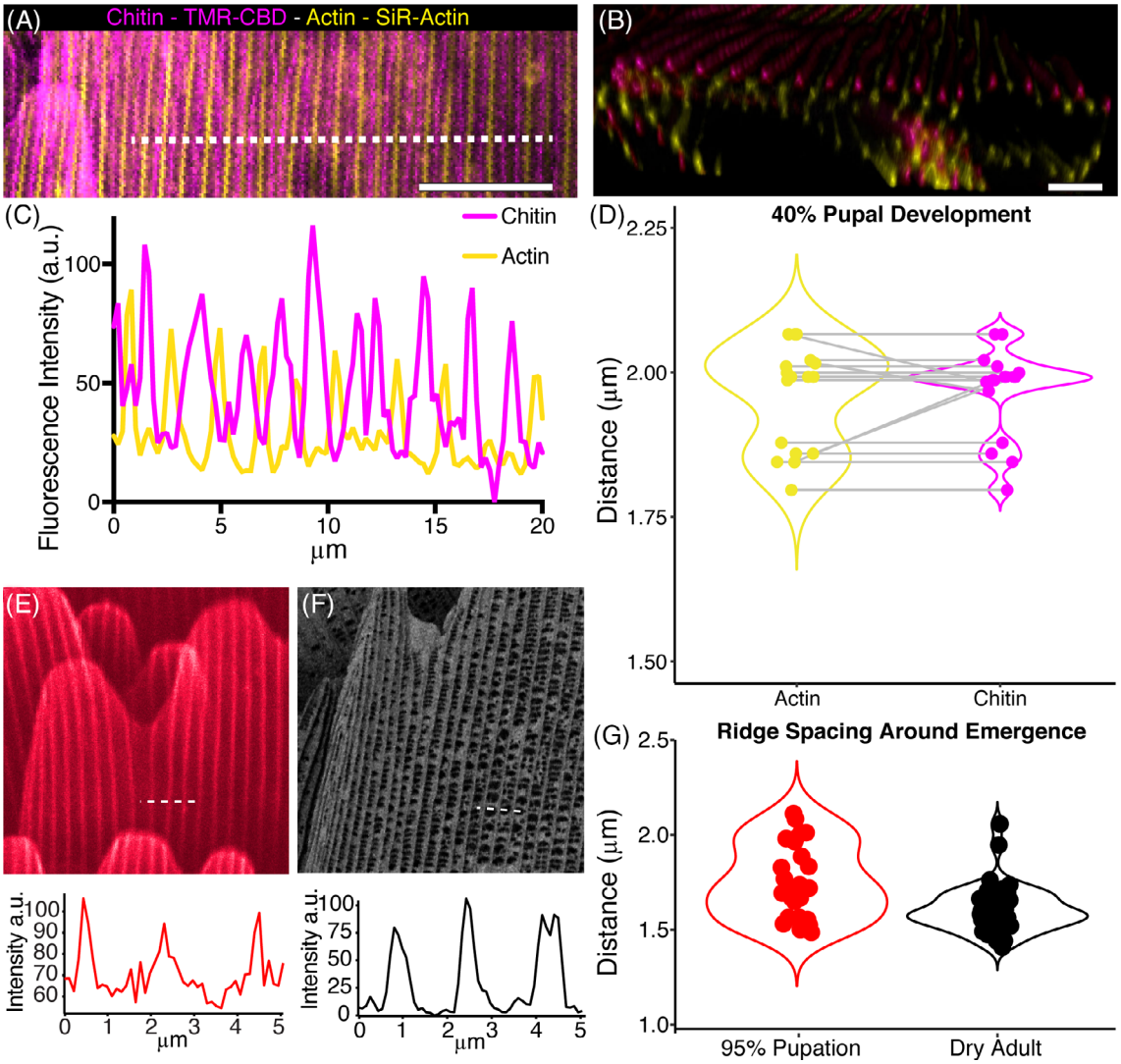

FIGURE 2 Adult inter-ridge distances are pre-established by actin and chitin deposition sites. A, Confocal microscopy of F-actin (yellow) and chitin (magenta) stainings in dorsal forewing scales at 40% pupal development. Chitin-positive signals corresponds to presumptive ridges. B, A 3D reconstruction of a confocal stack of actin (yellow) and chitin (magenta) stains in scales at 40% pupal development. C, Fluorescence intensity trace of F-actin and chitin fluorescence derived from dotted line in panel A. D, Average spacing between F-actin bundles and chitin deposition sites extracted by Fourier transform on 17 scales, averaging 20 measurements per scale in both channels. Actin and chitin spacings from the same intensity trace are connected by gray lines. E, Chitin autofluorescence image from a late stage pupa and intensity trace derived from dotted line. F, SEM of adult scale and extracted intensity trace (gray value) derived from dotted line. G, Quantification of chitin ridge spacing in late pupal development and adult scales. Scale bars = 10 µm in A, B

scales. In contrast, scanning electron microscopes are becoming more suitable for automated acquisition of high resolution images from large areas. We took advantage of this technological development to develop a phenomics approach to the problem of ultrastructural variation, and took the challenge to phenotype one of the more intricate pattern elements of the *V. cardui* wings, the Cu1-Cu2 eyespot from the ventral hindwing (Figure 1C). First, we devised a workflow written in R that facilitates the semi-automatic measurement of 11 ultrastructural variables from SEM images. We dubbed this package *SEMolina*, reflecting its use of "granular" pixel gray values from SEM images. In this workflow, the experimenter manually and carefully draws line segments that transect the scale ridges and cross ribs in Fiji, generating two perpendicular traces of pixel intensity values (Figure 4). The *SEMolina* tools implement Fourier transforms and peak calling rules to derive multiple variables (see Experimental Procedures section): ridge spacing, ridge width, crossrib spacing, and crossrib width (Table 1). Because multiple ridges or crossribs are simultaneously measured from a single trace, a standard deviation (SD) can be computed in each individual scale for these four traits, yielding four additional variables.

Scale width is measured by the length of the inter-ridge transect, as we drew segments reaching both sides of the scale. The

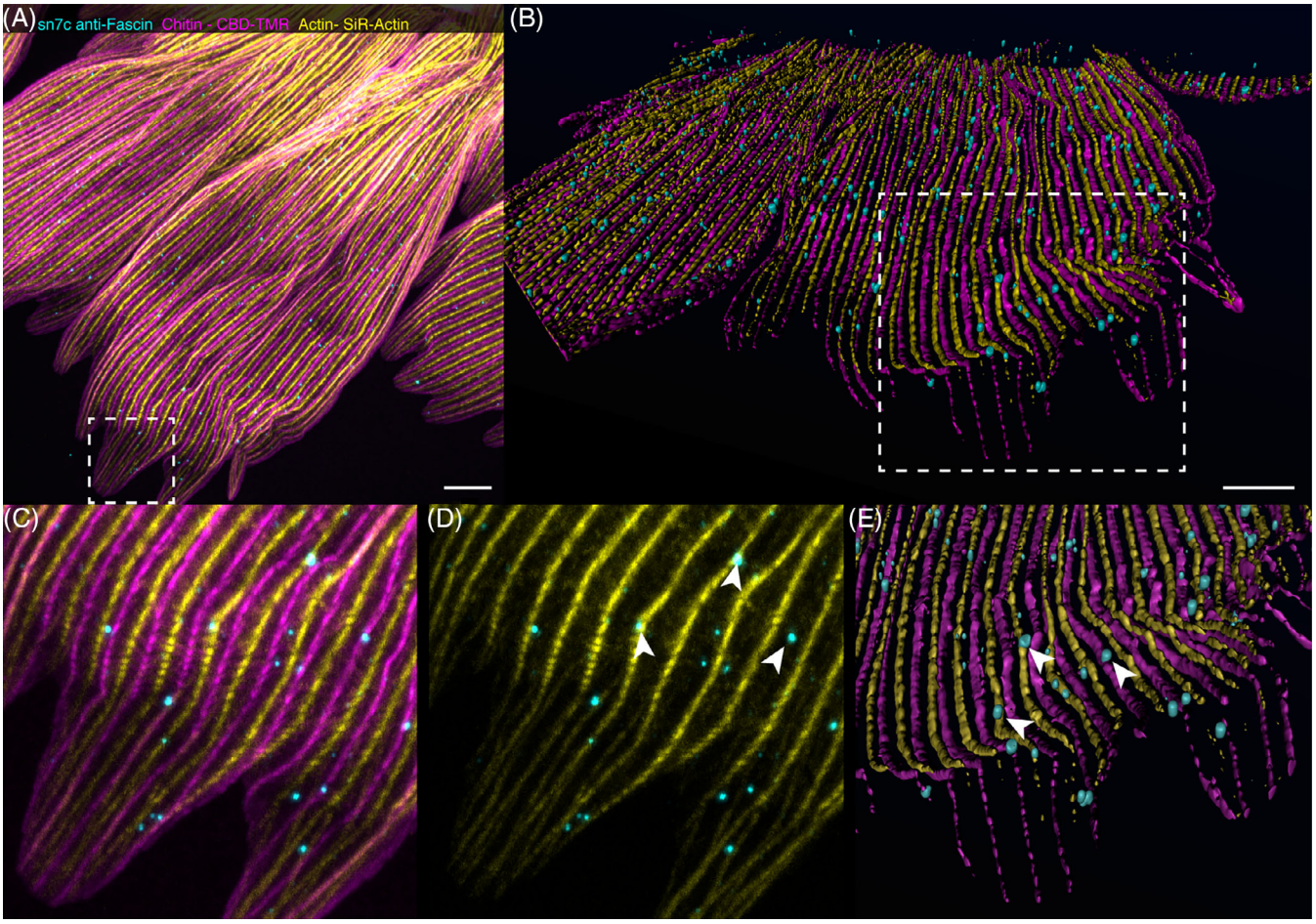

FIGURE 3 Cytoskeletal patterning of scale ridges in mid-pupae. A, Confocal microscopy of F-actin (SiR-actin, yellow), chitin (CBD-TMR, magenta) and Fascin (sn7c mAb, cyan) stainings in dorsal forewing scales at 40% pupal development. Chitin-positive signals correspond to presumptive ridges. B, 3D reconstruction of a confocal acquisition from the same triple-stained tissue. C,D, Inset corresponding to dotted box from panel A, with (panel C) and without (panel D) the chitin staining. Arrowheads: Singed/Fascin aggregates. E, Inset corresponding to the dotted box from panel B. Arrowheads: Singed/Fascin aggregates localize around F-actin bundles. Scale bars = 10 μm in A, B

level of cuticular filling between cross-ribs, recently called "ectopic lamina,"[36] is measured by mean gray values. Second, we imaged at high-resolution the entire eyespot using built-in automated acquisition software from a digital microscope, providing color information at a single-scale resolution (individual images captured at 300×), and from an SEM providing ultrastructural details of the scale surfaces (individual images captured at 300× with an effective pixel size of 67 nm). We isolated 1161 cover scales from this overlay (sub-sample shown in Figure 5A,B), recorded their XY-coordinates, and assigned them one of seven scale type categories depending on color and eyespot ring position (Figure 5C).

2.3 | Clustering analysis reveals correlation between color and structure

A rapid visual assessment of magnified SEM views suggested there were five ultrastructural types in the eyespot pattern (Figure 5D). However, the subjectivity of this classification begged for a more systematic test. Thus, we applied the ultrastructural measurement method, implementing SEMolina to measure 11 traits across 1,161 scales from the Cu1-Cu2 eyespot (Figure 6A). A principal component analysis (PCA) of the total data revealed that scale ultrastructures cluster by scale color (Figure 6B), with the first two components accounting for 53.5% of the variation (PC1 33.65% and PC2 19.84%). While we initially split the brown-beige scales on either side of the eyespot black ring as distinct by position, those scales were indistinguishable from each other (b vs d, multivariate analysis of variance [MANOVA], $P = 0.315$).

Similarly, blue and turquoise scales at the center of the eyespot could not be distinguished (f vs g, MANOVA, $P = 0.063$), consistently with the idea that blue-range scale color nuances, in the *Vanessa* genus and other nymphalids, derive from scale stacking and scale thickness effects that

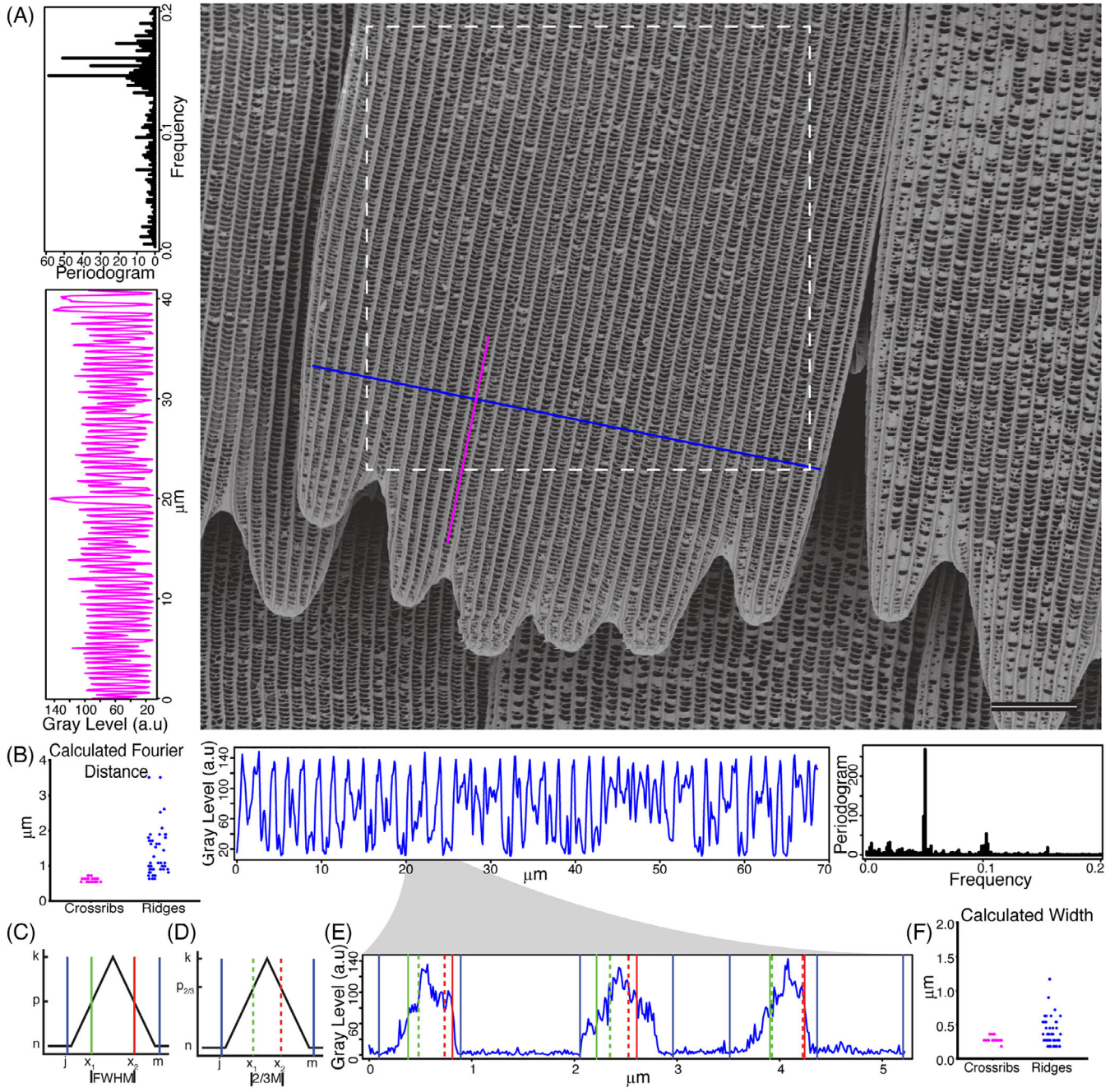

FIGURE 4 SEM-based methods for measuring spacing and widths of ridges and crossribs. A, A representative black scale from a *V. cardui* Cu2 eyespot with a trace of ridges (blue) and crossribs (magenta) with resulting periodograms. Dashed box: area used to calculate gray values. B, For the scale in panel A, we report a spacing mode of 1.77 µm ± 0.68 µm between ridges and 0.62 µm ± 0.06 µm between crossribs. C,D, Graphical representations of the variables used for peak width calculation; a WM = 0.5 (ie, 1/2 of the *k-n* amplitude) corresponds to a classical FWHM measurements (panel C) but did not match width features on our samples; a WM = 0.67 (ie, 2/3 of the *k-n* amplitude) was used for ridge and crossrib width measurements (panel D). E, Magnified view of an inter-ridge trace. Dotted red and green lines represent the computed ridge width intervals with WM = 0.67. F, For the scale in panel A, we report a mean ridge width of 0.39 µm ± 0.21 µm, and 0.28 µm ± 0.06 µm crossribs (not shown here in magnified view). Scale bar A = 10 µm

could not be measured here.[17] All other scale types were statistically different (MANOVA, $0.021 < P < 0.043$). This clustering demonstrates the existence of discrete ultrastructural types within the eyespot pattern. In this specific pattern element, we could delineate the existence of five discrete types of cover scales (as in Figure 5D): vein-covering beige (type a in our initial categorization), brown-beige (b and d), melanic (c), orange (e), and blue-turquoise (f and g).

We calculated the highest contributors to PC1 and PC2 by percent contribution (Table 1) then dropped factors which contributed most to the variation in the PCA including crossrib width SD (Figure 6C-C′).

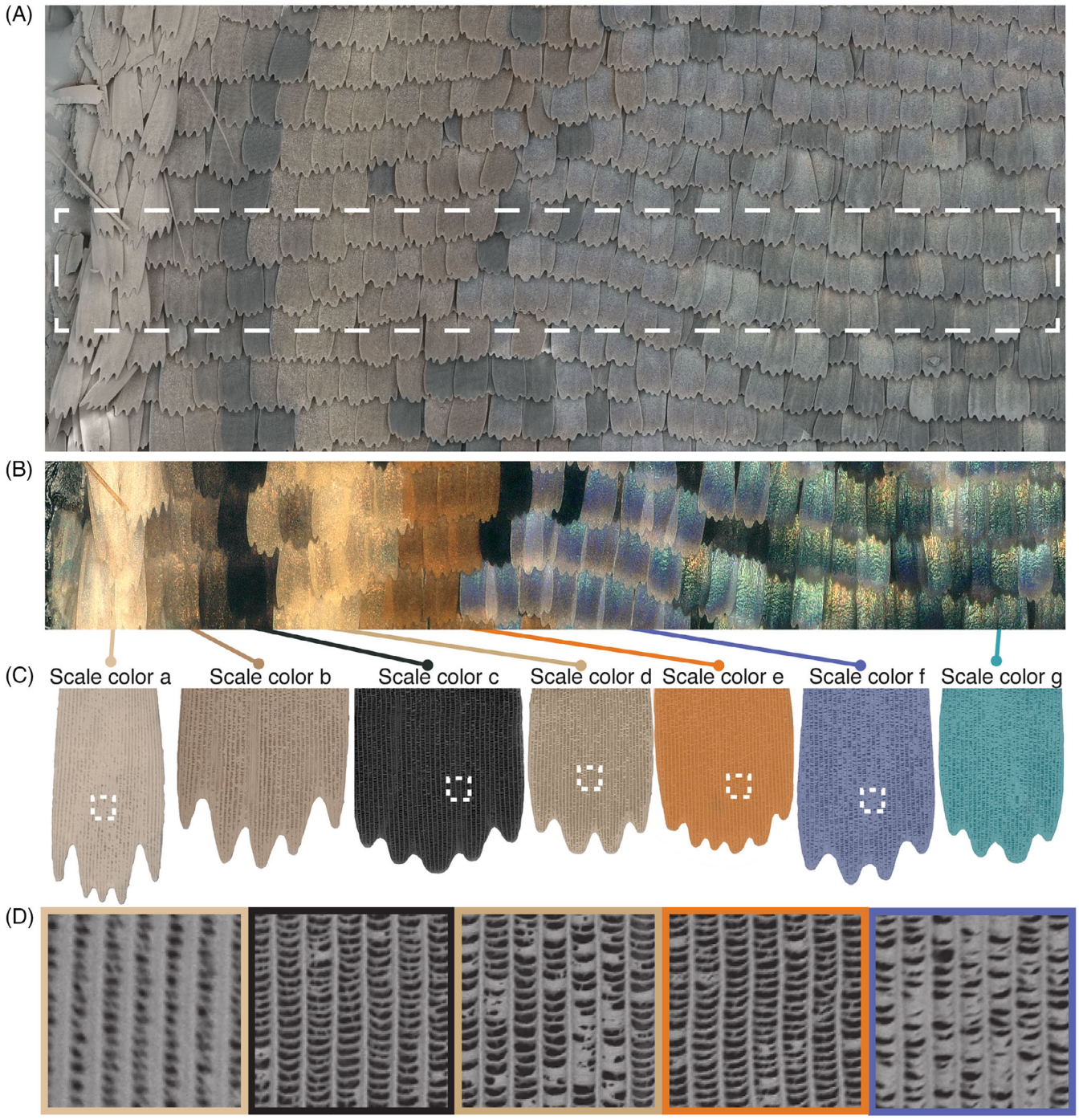

FIGURE 5 Initial categorization of the Cu1-Cu2 *V. cardui* eyespot into 7 scale types. A, Overlaid SEM micrograph with a corresponding light microscopy image. B, Light microscope image of a transect of the *V. cardui* eyespot showing all 7 scale colors. C, False colored SEM micrographs of representative scales of the corresponding color type. D, SEM micrographs taken from representative scales from panel C depicting the diversity of ultrastructures. Images are approximately 12 × 12 μm

Interesting inferences about scale type similarities can be drawn from the results of the PCA analysis. First, crossrib width SD (our proxy for order-disorder) is a powerful contributor to grouping by scale color. There is a range in observed order-disorder of crossrib widths, with blue/turquoise scales being more disordered, (broad density spread of within-scale SD, Figure 6C′), while by comparison black and orange scales appear highly ordered, having low crossrib width SD.

Clustering by color was examined when this level was dropped, revealing that crossrib order-disorder was responsible for driving some of the cluster separation of the multiple brown color types (Figure 6D). In addition, inter-crossrib spacing also contributed to the separation between two brown scale types.

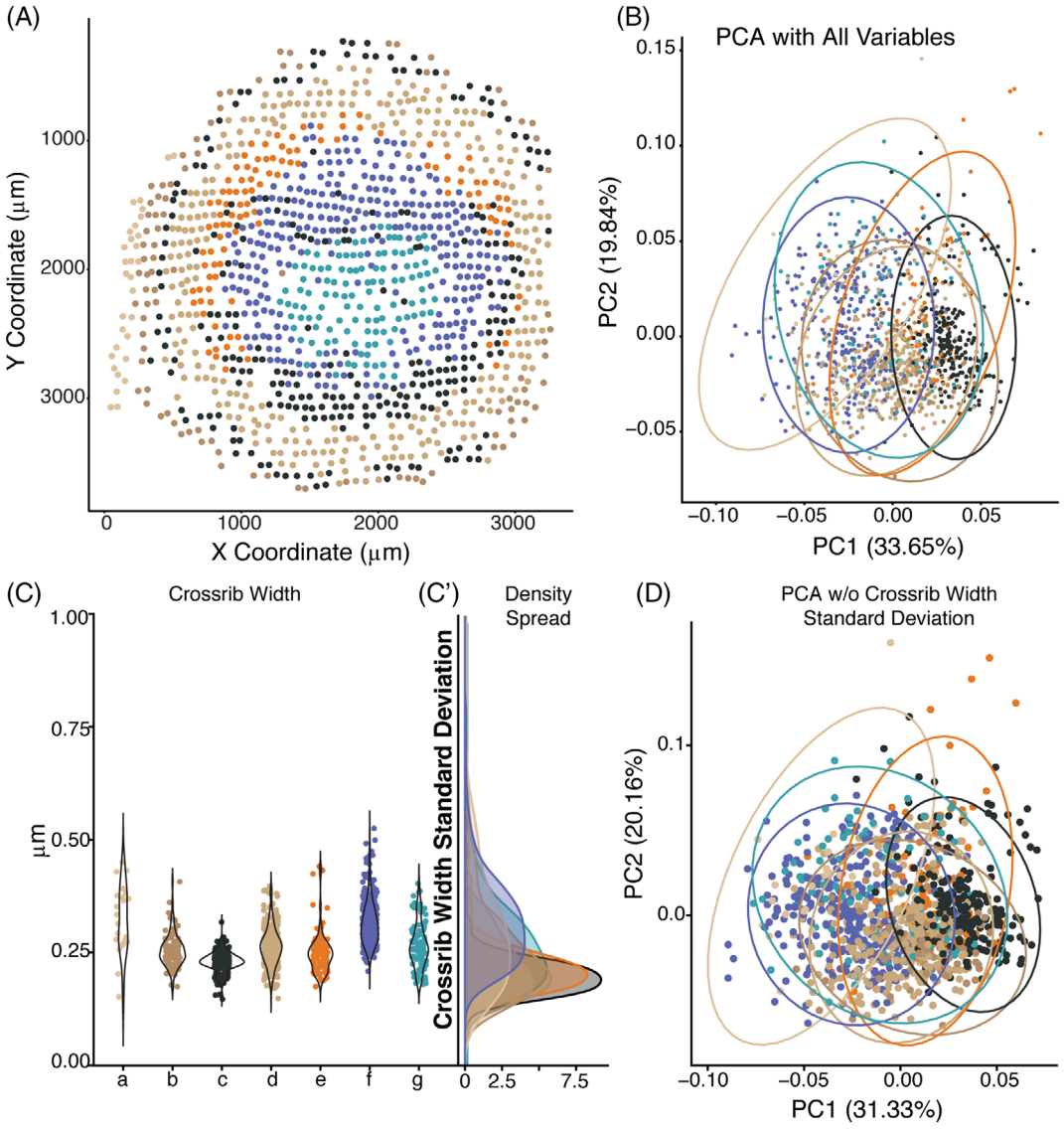

FIGURE 6 Continuous variation and clustering of ultrastructural variation by scale color. Each panel corresponds to a dataset of eyespot cover scales measured using *SEMolina*. A, Position and scale color assignment of the 1,161 scales; plotting individual scales X and Y coordinate and color category reconstitute the ventral Cu1-Cu2 eyespot. B, PC1 plotted against PC2 of the PCA; each ellipse surrounds a color group, and represents the area of component space which the cluster of points occupies with a 95% confidence interval. C-C′, Distribution by scale types of mean crossrib widths (panel C), and density plots of their SDs (panel C′) D, PC1 plotted against PC2 of the PCA run on 10 (not including crossrib width SD) measurements from 1,161 scales

Dropping ridge width increased clustering between multiple color types. Additionally, clustering of scale ultrastructures based on proximodistal position was observed. However, this correlation could not be completely disentangled from changes in proportion of scale colors along the proximodistal axis.

3 | DISCUSSION

3.1 | Continuity between developmental cytoskeletal patterns and adult ultrastructures

We followed up on a previous study of scale developmental dynamics[30] and found additional support for an active role of the cytoskeleton in patterning the spacing of the presumptive scale ridges. Indeed, the alternation of F-actin bundles and chitin-deposition sites show consistent periodicity from 40% to 95% of pupal development. Following adult emergence and wing drying, while scales may contract slightly, inter-ridge distances match their developmental counterparts. In the expanded eyespot analysis of SEM data, we observed a highly repeatable periodicity of inter-ridge distances within scale types, as well as the subtle differences between color scale types. Fascin/Singed and other actin-bundling factors that are classically studied in *Drosophila* bristles[44-48] could be key factors in the control of these key parameters, and will require further investigation in Lepidoptera. We also expect microtubules

TABLE 1 Contributions to PC1 and PC2 shown as percents, a weighted average was calculated for the contribution of each measure to PC1 and PC2[a]

Explained Variation (%)	PC1 33.65%	PC2 19.84%	Weighted PC1+PC2
CR Width SD	18.24	5.27	13.43
CR Distance	12.72	11.08	12.11
R Width	6.20	20.60	11.54
CR Distance SD	14.10	7.10	11.50
CR Width	16.95	1.31	11.15
Mean Gray	11.53	9.32	10.71
R Width SD	8.97	7.35	8.37
Scale Width	0.12	20.77	7.78
R Distance SD	5.96	9.24	7.17
R Distance	4.01	4.73	4.28
Number of Serrations	1.19	3.23	1.95

[a]The top 3 contributing factors were crossrib width standard deviation, crossrib spacing, and ridge width.

to interact with the actin network and to play an active role in this process, as they do during *Drosophila* bristle development.[49,50] Indeed, microtubules have been described to take a fan-like appearance in electronic microscopy sections performed during scale flattening in Lepidoptera,[51] and it will be interesting to document microtubule dynamics using fluorescent stainings.

3.2 | Scale morphological diversity across a single color pattern

Our semi-automated pipeline allowed a comprehensive analysis of scale structure in a single pattern element, and this type of analysis could be repurposed to high-throughput comparative analyses of many individuals or species. Our PCA reveals that scale structural variations cluster by color, confirming previous reports that highlighted an interdependency between pigment composition and ultrastructure.[34-36] Despite the strong correlates between structure and color, scale structures did not fall into discrete classes or types in the eyespot sample, and it would not always be possible to predict the color of a scale based solely on its structure. Nonetheless, crossrib width SD, crossrib spacing and ridge width accounted for roughly 37% of the variation in the first two PCs. Indicating that crossrib orderedness is a key component of scale type diversity.

Of interest, our phenotyping method identified specific ultrastructural features that distinguish melanic scales. These scales appear matte black, and are thus functionally tuned for anti-reflectance. Other reports have studied the biophysics of light-trapping by analogous scale structures, and converge in the finding that highly ordered structures are required for light manipulation.[10,11,52,53] Our measurements of over 250 black scales recapitulate the finding that orderedness of scale ultrastructures, particularly crossrib width and spacing, is linked to light trapping in matte black scale types.

3.3 | Limitations of the semi-automated measurement method

The workflow outlined is best performed on high-quality images, if possible generated with a recent SEM instrument capable of automatedly imaging large areas. It is also important to mention that the technique is inherently limited by the quality and features of the SEM acquisition. Unless they are physically removed, only cover scales can be phenotyped from this bird's-eye view; here, we excluded the few ground scales that were exposed in our analysis. Additionally, it is not possible to measure trabeculae or lamina thickness with SEM without freeze-fracturing the scales,[54,55] which is impracticable for reaching large sample sizes. Also because scales were measured in situ and not removed from the wing, it was not possible to calculate measures such as scale length, ratio, area or total shape, all of which may have been informative features of scale structure. Finally, given the resolution of imaging in the current analysis, we had an effective pixel size of 67 nm. With this resolution, we cannot reasonably contour features <135 nm (ie, < 2 pixels) and if finer scale measurements were desired, an increased magnification would be required at the cost of total scanning time. Experimenters interested in the workflow must thus find a trade-off between spatial resolution and the size of their region of interest, depending on how much time can be allocated to imaging.

Finally, it is important to highlight that the ability of the procedure to accurately measure features depends on how contrasted the ultrastructural features appear on the analyzed images. The use of an SEM back-scattered electron detector can help in creating contrast, which allowed for better peak calling. The *SEMolina* pipeline was subjected to a rigorous validation step where automated measurements were compared with hand measurements from the same scale (Figure 7). During validation, we inserted a width multiplier (WM) correction factor to more accurately call ridge widths. The major limitation of our current data set in the pixel size. The full-width at half-maximum function requires multiple pixels to call a width; hence, as the WM is increased above 0.5 (half-maximum factor of the FWHM), fewer pixels are incorporated into the interval, which can result in the peak not being called by the program. For any analysis, we recommend using a validation step comparing *SEMolina* with measures made manually.

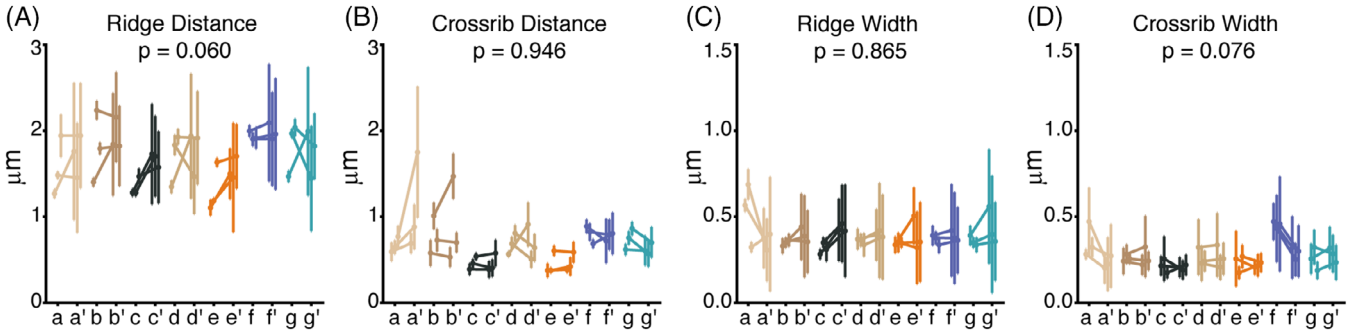

FIGURE 7 Validation of the *SEMolina* method with manual measurements. A-D, Comparison of manual (no apostrophes) and semi-automated (apostrophe letters) measurements in 3 scales per scale type ($N = 21$ scales in total). For each scale, mean measurements are derived from 5 replicates for manual methods, are paired between methods (horizontal bars), and are shown with their SDs (vertical bars). P-values are given for Wilcoxon signed-rank tests performed on 21 scales, testing for differences between the manual and semi-automated methods. A, Ridge distance. B, Crossrib distance. C, Ridge width. D, Crossrib width

3.4 | Potential for comparative phenomics, transcriptomics, and reverse genetics

By using the SEMolina workflow on a large 2D SEM image, a single experimenter can extract information from hundreds of lepidopteran scales per day. The data set here represents 11 measurements for 1161 scales. Assuming roughly 40 ridges and 40 crossribs were measured per scale this data set represents almost 200 000 individual measurements. The relative ease and speed of the *SEMolina* pipeline as well as the potential to generate massive datasets provides a valuable tool for generating phenomic data.

Here, we implemented the method on a single eyespot pattern, and it will be interesting to use the method for comparing various wing regions, experimental conditions, natural populations, or species, depending on the biological question of interest. For instance, the butterfly genus *Eumaeus* (Theclinae: Lycaenidae) displays a variety of iridescent patches with colors ranging from bright yellow to green, turquoise, cyan, blue, and violet. Preliminary SEM of a single iridescent scale of *Eumaeus childrenae* suggests that variations in a diffraction grating structure may explain the biophotonic continuum observed within the six *Eumaeus* species,[15] and the regularity of these ultrastructures make them well-suited for the SEMolina workflow. The phenomics approach could also be coupled with single-cell transcriptomics, in an attempt to match differential gene expression during scale development with scale morphologies. The *V. cardui* eyespot we studied here shows regionalized expression of the transcription factors Distal-less, Engrailed/Invected (En/Inv), and Spalt as early as the stage of scale cell precursor differentiation, around 18 hr after pupation.[56]

Thus, it can be expected that the scale cell precursors from different eyespot rings maintain differential expression in the following stages, and the combination of single-cell transcriptomics with single-scale phenomics could yield interesting insights on the gene regulatory networks that lead scale cells toward distinct morphologies. The workflow can also be used in combination with reverse genetics approach; indeed, CRISPR knock-outs of candidate wing patterning genes generate mosaic mutant clones with sharp boundaries,[36,57-61] at least when the targeted genes have a cell autonomous function. For instance, knock-outs of the *optix* transcription factor affects both pigment composition and structural coloration, suggesting a master role for scale identity.[62] We suggest that high-throughput phenotyping of CRISPR mutant clones will be a valuable tool for understanding the gene-to-phenotype relationships that have given rise to the diversity of lepidopteran color patterns.

4 | CONCLUSION

Understanding how insect epithelia differentiate, and deploy internal mechanisms such as the cytoskeleton to build complex ultrastructures, is an interesting challenge for cellular and developmental biology. Here we described two new reagents (TMR-CBD and the sn7C monoclonal antibody) that will be ideal for future studies of insect epithelial morphogenesis, and provide measurements that buttress the previously proposed continuity between the developing scale cytoskeleton and the adult ultrastructures. Then, we devised a novel method for characterizing the adult ultrastructures from large SEM images, and were able to implement a phenomics approach on an entire large pattern using approximately 200 000 individual measurements taken across 1161 individual scales. While this multicolor element revealed relatively homogenous scale morphologies, multivariate statistical analysis could distinguish up to 5 ultrastructural scale types. Crossrib parameters such as average distance, or the variability in filling across a scale (width SD) where the main contributors to these nuances and reveal that both black

and orange scales showed light-trapping features compared with more reflective scales. Overall, the aggressive morphometrics approach describe here on the butterfly wing pattern system allows a clear characterization of single-cell phenotypes, and opens new opportunities to connect observable levels of cellular variation with molecular data from the single-cell sequencing revolution.

5 | EXPERIMENTAL PROCEDURES

5.1 | Insect rearing and developmental tissue preparation

Vanessa cardui caterpillars (Carolina Biological Supply) were reared in plastic containers placed at 25°C and 55% relative humidity. Time of pupation was monitored every two hours, and pupae were dissected at 48 hr (~40% of total pupal development) for dissection. Pupae were dissected in ice cold phosphate buffered saline (PBS) and whole wings removed and immediately fixed at room temperature in fixative (PBS, 3.7% formaldehyde, 2 mM EGTA [ethylene glycol-bis(β-aminoethyl ether)-N,N,N′,N′-tetraacetic acid]) for 30 min. Following successive washes in PBS, wings were blocked in PT-BSA (PBS, 4% Triton X-100, 0.5% bovine serum albumin [BSA]) for >2 hr, and incubated in PT-BSA with a 1:5 dilution of sn7c monoclonal mouse serum (Developmental Studies Hybridoma Bank) directed against the *Drosophila* singed homolog of Fascin,[43] overnight at 4°C. The wings were then washed in PT 4% (PBS, 4% Triton X-100), incubated with 1:200 dilution of anti-mouse AlexaFluor488 secondary antibody (Thermo Fisher) at room temperature for 2 hr, washed in PT 4%, transferred to PT (PBS, 0.1% Triton X-100), incubated with a 1:100 dilution (5 μg/mL final concentration) of TMR-Star Conjugated Chitin-Binding Probe (542 nm, TMR-CBD, New England Biolabs, reagent obtained by special request to the manufacturer) for 3-6 hr at room temperature, and washed with PT. Finally, the wings were incubated with 100 nM of SiR-Actin (652 nm, Cytoskeleton Inc.) overnight at 4°C, washed in PT, counterstained in 50% glycerol:PBS with 1 μg/mL DAPI (4′,6-diamidine-2-phenylidole-dihydrochloride) for >30 min, and stored in 60% glycerol:PBS at 4°C.

5.1.1 | Confocal imaging

Wings were mounted on glass slides in 60% glycerol:PBS, covered with a #1.5 thickness coverslip, and sealed with nail polish. Images were collected using an Olympus FV1200 confocal microscope mounted with an 60x Apochromat oil-immersion objective. Images of structures of interest were collected at non-saturating conditions. Z steps were taken $\Delta z = 0.47$ μm and resulting Z stacks were either max-projected for analysis in ImageJ/FIJI[63] or 3D-reconstructed using the Imaris 3D/4D visualization software. Pupal wing autofluorescence was imaged using an Olympus IX71 microscope equipped with a 60× 1.2 numerical aperture water-immersion objective lens. The confocal pin holes were set to 50 μm and optimized for the detectors in both channels. The samples were illuminated with a 5 mW 448 nm diode laser and the emitted signal was routed by a 568-nm long-pass beam splitter to either the 500/60 nm or 609/53 nm band-pass emission filters, and the signals were detected using two identical avalanche photodiodes (APD).

5.1.2 | Whole insect specimen preparation

A *V. cardui* butterfly specimen was frozen at −20°C for 24 hr, spread ventral-side up on a flat mounting board, and let to dry for 4 days.

5.1.3 | Microphotography

A full *V. cardui* butterfly was imaged with a Keyence VHX-5000 digital microscope mounted with a VH-Z00R lens set-up at 50× magnification, and using the built-in 3D stitching software (Figure 1A). The forewing and hindwing regions of interest were then excised, mounted with the ventral side up onto carbon tape, and re-imaged with the VH-Z100R lens set-up at 300× magnification (Figure 1B,C).

5.1.4 | SEM

The Cu1-Cu2 sample was sputter coated with 12.5 nm of gold at 90°, and re-coated at 45° to provide homogenous conductivity. All scanning electron microscope images were taken using a FEI Teneo LV SEM instrument. A first low-magnification images of the entire Cu1-Cu2 eyespot was generated using secondary electrons with individual acquisitions at 300×, and the FEI Maps software piloting the automatic acquisition and stitching of overlapping areas. Then, using a similar stitching strategy, high-resolution segments of the eyespot were scanned using back-scattered electrons at a voltage of 5 kV, 1500× magnification, and a pixel size of 0.067 μm. Higher resolutions can be obtained with higher magnification at the cost of increased image number and scanning time for a given region of interest.

5.1.5 | SEM pixel profile acquisitions

The 300× micrograph and SEM image of the Cu1-Cu2 wing region were overlaid to register the color and positional information for each scale. Then, morphometric analyses were performed on the high-resolution images obtained from stitched 1500× micrographs. For each scale, one straight line segment was drawn across the full width of the scale,

perpendicular to the visible ridges and another perpendicular to the visible crossribs, using FIJI (Figure 2). Plots of the pixel gray values was extracted using the *plot profile* function. The pixel intensity profiles derived from the inter-ridge and inter-crossribs segments were then analysed using our custom *SEMolina* semi-automated pipeline to measure several ultrastructural features, as described below. All the *SEMolina* code is available on the GitHub repository at https://github.com/Hanliconius.

5.1.6 | Semi-automated measurements: ridges and crossribs

The extracted ridge trace (Figure 2A, blue) had local gray value maxima corresponding to the peaks of each ridge. This trace was Fourier-transformed using the TSA package in R, yielding the modal ridge spacing. (Figure 2A). The same process was applied to crossrib traces (Figure 2A, magenta). Individual ridge and crossrib spacings can be calculated SD were extracted (Figure 2B). For the ridge width calculation, a FWHM was applied to the trace. Valleys (blue vertical lines Figure 2C,D) were called where a minimum value was returned (n), and the maximum value between two valleys was called as k. A multiplier was applied the value between n and k to measure the peak width at a specified height. The result was called as p (width multiplier, WM) and was used to define x_1 and x_2. x_1 was called on the ascending side where the trace intersected p (green vertical lines) and x_2 was called on the descending side where the trace intersected p (red vertical lines). Ridge width was reported as the difference between x_1 and x_2 (Figure 2C-E). Ridge width was derived using automated peak width calculation was performed in R, and the calculation was calibrated to hand measurements taken from a small number of scales (Figure 7). Various WM were tested including 0.5 (Figure 2C), 0.67 (Figure 2D), and 0.7. A WM of $p = 0.67$ was used to calculate all ridge widths (Figure 2D). The same methods were applied to the crossrib traces to extract crossrib width, and after calibration, a WM of $p = 0.67$ was used to calculate all cross-rib widths.

5.1.7 | Semi-automated measurements: other scale features

The maximum × value from the inter-ridge segment was reported as the scale width, and scales where the full width of the scale could not be measured were not analysed. Ectopic lamina cover was quantified by drawing a rectangle over the exposed scale in FIJI (Figure 2A) and the mean gray value was extracted with the *measure* function. The serrations at the tip of each scale were manually counted. The XY coordinates of each scale were extracted in μm using FIJI, with the top left of the eyespot defining the origin (X = 0, Y = 0).

5.1.8 | Statistical multivariate analyses

Statistical significance of clustering by color was assessed in R using a MANOVA using the pairwise Adonis package and PCA was performed on log-transformed data using the ggfortify package. Contributions to PC1 and PC2 were extracted using the factoextra package.

ACKNOWLEDGMENTS

We thank the GW Nanofabrication and Imaging Center for enabling SEM, and in particular Christine Brantner and Anastas Popratiloff for their technical assistance; Richard Day for the chitin autofluorescence images; Patricia Hernandez for providing access to microscopes; Nipam Patel, Brian Counterman and Ryan Null for inspiring discussions on butterfly scale ultrastructures and imaging tips; and Huimin Chen for advice with automation of measurements. This research was funded by the GW Columbian College of Arts and Sciences, and the National Science Foundation awards IOS-1656553 and IOS-1755329 to A.M. C.R.D. and J.J.H. designed the study, contributed the image analysis workflow, performed the statistical analyses, and wrote the first draft of the manuscript; C.R.D. and A.R. performed image acquisition and analysis. C.R.D., J.J.H., and A.R. designed the manuscript Figures. A.M. supervised the research and contributed sections of the manuscript. All authors contributed to manuscript revision, read and approved the submitted version.

ORCID

Christopher R. Day https://orcid.org/0000-0002-1841-950X
Joseph J. Hanly https://orcid.org/0000-0002-9459-9776
Arnaud Martin https://orcid.org/0000-0002-5980-2249

REFERENCES

1. Burleigh G, Alphonse K, Alverson AJ, et al. Next-generation phenomics for the Tree of Life. *PLoS Curr*. 2013;5. http://currents.plos.org/treeoflife/index.html%3Fp=2583.html.
2. Deans AR, Lewis SE, Huala E, et al. Finding our way through phenotypes. *PLoS Biol*. 2015;13:e1002033.
3. Skelly DA, Merrihew GE, Riffle M, et al. Integrative phenomics reveals insight into the structure of phenotypic diversity in budding yeast. *Genome Res*. 2013;23:1496-1504.
4. Yvert G, Ohnuki S, Nogami S, et al. Single-cell phenomics reveals intra-species variation of phenotypic noise in yeast. *BMC Syst Biol*. 2013;7:54.
5. Nijhout HF. Smithsonian series in comparative evolutionary biology. *The Development and Evolution of Butterfly Wing Patterns*. Washington: Smithsonian Institution Press; 1991:297.
6. Ghiradella H. Light and color on the wing: structural colors in butterflies and moths. *Appl Optics*. 1991;30:3492-3500.

7. Sekimura T. An integrative approach to the analysis of pattern formation in butterfly wings: experiments and models. In: Capasso V, Gromov M, Harel-Bellan A, Morozova N, Pritchard LL, eds. *Pattern Formation in Morphogenesis*. Vol 15. Berlin, Heidelberg: Springer; 2013:121-136.
8. Lou S, Guo X, Fan T, Zhang D. Butterflies: inspiration for solar cells and sunlight water-splitting catalysts. *Energ Environ Sci*. 2012;5:9195.
9. Vukusic P, Sambles JR, Lawrence CR. Structurally assisted blackness in butterfly scales. *Proc Biol Sci*. 2004;271(Suppl 4):S237-S239.
10. Wang W, Zhang W, Zhang D, Wang GP. A low-cost, high-efficiency light absorption structure inspired by the Papilio ulysses butterfly. *RSC Adv*. 2017;7:22749-22756.
11. Zhao Q, Guo X, Fan T, Ding J, Zhang D, Guo Q. Art of blackness in butterfly wings as natural solar collector. *Soft Matter*. 2011;7:11433.
12. Sweeney A, Jiggins C, Johnsen S. Polarized light as a butterfly mating signal: insect communication. *Nature*. 2003;423:31-32.
13. Vukusic P, Kelly R, Hooper I. A biological sub-micron thickness optical broadband reflector characterized using both light and microwaves. *J R Soc Interface*. 2009;6:S193-S201.
14. Narasimhan V, Siddique RH, Lee JO, et al. Multifunctional biophotonic nanostructures inspired by the longtail glasswing butterfly for medical devices. *Nat Nanotechnol*. 2018;13:512-519.
15. Ingram AL, Parker AR. A review of the diversity and evolution of photonic structures in butterflies, incorporating the work of John Huxley (The Natural History Museum, London from 1961 to 1990). *Philos Trans R Soc Lond B Biol Sci*. 2008;363:2465-2480.
16. Parnell AJ, Bradford JE, Curran EV, et al. Wing scale ultrastructure underlying convergent and divergent iridescent colours in mimetic *Heliconius* butterflies. *J R Soc Interface*. 2018;15:20170948.
17. Stavenga DG, Leertouwer HL, Wilts BD. Coloration principles of nymphaline butterflies - thin films, melanin, ommochromes and wing scale stacking. *J Exp Biol*. 2014;217:2171-2180.
18. Thayer RC, Allen FI, Patel NH. Structural color in *Junonia* butterflies evolves by tuning scale lamina thickness. 2019. http://biorxiv.org/lookup/doi/10.1101/584532. Accessed May 26, 2019.
19. Wilts BD, Matsushita A, Arikawa K, Stavenga DG. Spectrally tuned structural and pigmentary coloration of birdwing butterfly wing scales. *J R Soc Interface*. 2015;12:20150717.
20. Kinoshita S, Yoshioka S. Structural colors in nature: the role of regularity and irregularity in the structure. *ChemPhysChem*. 2005;6:1442-1459.
21. Kinoshita S, Yoshioka S, Fujii Y, Okamoto N. Photophysics of structural color in the morpho butterflies. *Forma*. 2002;17:103-121.
22. Vukusic P, Sambles JR, Lawrence CR, Wootton RJ. Quantified interference and diffraction in single Morpho butterfly scales. *Proc R Soc Lond B Biol Sci*. 1999;266:1403-1411.
23. Wang W, Zhang W, Gu J, et al. Design of a structure with low incident and viewing angle dependence inspired by Morpho butterflies. *Sci Rep*. 2013;3:3427.
24. Kemp DJ, Vukusic P, Rutowski RL. Stress-mediated covariance between nano-structural architecture and ultraviolet butterfly coloration. *Funct Ecol*. 2006;20:282-289.
25. Wilts BD, Apeleo Zubiri B, Klatt MA, et al. Butterfly gyroid nanostructures as a time-frozen glimpse of intracellular membrane development. *Sci Adv*. 2017;3:e1603119.
26. Boppré M, Vane-Wright RI. Androconial systems in Danainae (Lepidoptera): functional morphology of Amauris, Danaus, Tirumala and Euploea. *Zool J Linn Soc*. 1989;97:101-133.
27. Harvey DJ, Hall JPW. Phylogenetic revision of the Charis cleonus complex (Lepidoptera: Riodinidae): revision of Charis cleonus complex. *Syst Entomol*. 2002;27:265-300.
28. Iwata M, Ohno Y, Otaki JM. Real-time in vivo imaging of butterfly wing development: revealing the cellular dynamics of the pupal wing tissue. Ed by Joshua B Benoit. *PLoS One*. 2014;9:e89500.
29. Ohno Y, Otaki JM. Live Cell Imaging of Butterfly Pupal and Larval Wings In Vivo. *PLos One*. 2015;10:e0128332.
30. Dinwiddie A, Null R, Pizzano M, et al. Dynamics of F-actin prefigure the structure of butterfly wing scales. *Dev Biol*. 2014;392:404-418.
31. Nardi JB, Magee-Adams SM. Formation of scale spacing patterns in a moth wing. *Dev Biol*. 1986;116:278-290.
32. Ghiradella H. Hairs, bristles and scales. *Microscopic Anatomy of Invertebrates*. Vol 11A. New York, NY: Wiley-Liss; 1998:257-287.
33. Ghiradella HT, Butler MW. Many variations on a few themes: a broader look at development of iridescent scales (and feathers). *J R Soc Interface*. 2009;6:S243-S251.
34. Gilbert LE, Forrest HS, Schultz TD, Harvey DJ. Correlations of ultrastructure and pigmentation suggest how genes control development of wing scales of Heliconius butterflies. *J Res Lepid*. 1988;26:141-160.
35. Janssen JM, Monteiro A, Brakefield PM. Correlations between scale structure and pigmentation in butterfly wings. *Evol Dev*. 2001;3:415-423.
36. Matsuoka Y, Monteiro A. Melanin pathway genes regulate color and morphology of butterfly wing scales. *Cell Rep*. 2018;24:56-65.
37. Noh MY, Muthukrishnan S, Kramer KJ, Arakane Y. Cuticle formation and pigmentation in beetles. *Curr Opin Insect Sci*. 2016;17:1-9.
38. Sugumaran M, Barek H. Critical analysis of the melanogenic pathway in insects and higher animals. *Int J Mol Sci*. 2016;17:1753.
39. Binetti VR, Schiffman JD, Leaffer OD, Spanier JE, Schauer CL. The natural transparency and piezoelectric response of the Greta oto butterfly wing. *Integr Biol*. 2009;1:324-329.
40. Gruverman A, Rodriguez BJ, Kalinin SV. Nanoscale electromechanical and mechanical imaging of butterfly wings by scanning probe microscopy. *J Scan Probe Microsc*. 2006;1:74-78.
41. Brien MN, Enciso-Romero J, Parnell AJ, et al. Phenotypic variation in *Heliconius erato* crosses shows that iridescent structural colour is sex-linked and controlled by multiple genes. *Interface Focus*. 2019;9:20180047.
42. Saranathan V, Osuji CO, Mochrie SGJ, et al. Structure, function, and self-assembly of single network gyroid (I4132) photonic crystals in butterfly wing scales. *Proc Natl Acad Sci U S A*. 2010;107:11676-11681.
43. Cant K. Drosophila singed, a fascin homolog, is required for actin bundle formation during oogenesis and bristle extension. *J Cell Biol*. 1994;125:369-380.
44. Otani T, Ogura Y, Misaki K, et al. IKKε inhibits PKC to promote Fascin-dependent actin bundling. *Development*. 2016;143:3806-3816.
45. Bitan A, Rosenbaum I, Abdu U. Stable and dynamic microtubules coordinately determine and maintain Drosophila bristle shape. *Development*. 2012;139:1987-1996.
46. Nagaraj R, Adler PN. Dusky-like functions as a Rab11 effector for the deposition of cuticle during Drosophila bristle development. *Development*. 2012;139:906-916.

47. Shapira S, Bakhrat A, Bitan A, Abdu U. The Drosophila javelin Gene Encodes a Novel Actin-Associated Protein Required for Actin Assembly in the Bristle. *Mol Cell Biol*. 2011;31:4582-4592.
48. Wu J, Wang H, Guo X, Chen J. Cofilin-mediated actin dynamics promotes actin bundle formation during *Drosophila* bristle development. *Mol Biol Cell*. 2016;27:2554-2564.
49. Geng W, He B, Wang M, Adler PN. The tricornered gene, which is required for the integrity of epidermal cell extensions, encodes the Drosophila nuclear DBF2-related kinase. *Genetics*. 2000;156:1817-1828.
50. Goode BL, Drubin DG, Barnes G. Functional cooperation between the microtubule and actin cytoskeletons. *Curr Opin Cell Biol*. 2000;12:63-71.
51. Overton J. Microtubules and microfibrils in morphogenesis of the scale cells of Ephestia kühniella. *J Cell Biol*. 1966;29:293-305.
52. Han Z, Niu S, Shang C, Liu Z, Ren L. Light trapping structures in wing scales of butterfly Trogonoptera brookiana. *Nanoscale*. 2012;4:2879.
53. Sackey J, Berthier S, Maaza M, Beuvier T, Gibaud A. Comparative study on nanostructured order-disorder in the wing eyespots of the giant owl butterfly. *Caligo memnon IET Nanobiotechnol*. 2018;12:951-955.
54. Ghiradella H. Structure and development of iridescent butterfly scales: lattices and laminae. *J Morphol*. 1989;202:69-88.
55. Prum RO, Quinn T, Torres RH. Anatomically diverse butterfly scales all produce structural colours by coherent scattering. *J Exp Biol*. 2006;209:748-765.
56. Brunetti CR, Selegue JE, Monteiro A, French V, Brakefield PM, Carroll SB. The generation and diversification of butterfly eyespot color patterns. *Curr Biol*. 2001;11:1578-1585.
57. Connahs H, Tlili S, van Creij J, et al. Activation of butterfly eyespots by Distal-less is consistent with a reaction-diffusion process. *Development*. 2019;146:dev169367. http://biorxiv.org/lookup/doi/10.1101/183491.
58. Livraghi L, Martin A, Gibbs M, Braak N, Arif S, Breuker CJ. CRISPR/Cas9 as the key to unlocking the secrets of butterfly wing pattern development and its evolution. *Advances in Insect Physiology*. Vol 54. Amsterdam: Elsevier; 2018:85-115. https://linkinghub.elsevier.com/retrieve/pii/S0065280617300346.
59. Prakash A, Monteiro A. *apterous A* specifies dorsal wing patterns and sexual traits in butterflies. *Proc R Soc B Biol Sci*. 2018;285:20172685.
60. Westerman EL, VanKuren NW, Massardo D, et al. Aristaless controls butterfly wing color variation used in mimicry and mate choice. *Curr Biol*. 2018;28:3469-3474.e4.
61. Woronik A, Tunstrom K, Perry MW, et al. A female alternative life-history strategy arose via novel recruitment of homeobox gene, BarH-1. *bioRxiv*. 2018. http://biorxiv.org/lookup/doi/10.1101/424879. Accessed May 26, 2019.
62. Zhang L, Mazo-Vargas A, Reed RD. Single master regulatory gene coordinates the evolution and development of butterfly color and iridescence. *Proc Natl Acad Sci U S A*. 2017;114:10707-10712.
63. Schindelin J, Arganda-Carreras I, Frise E, et al. Fiji: an open-source platform for biological-image analysis. *Nat Methods*. 2012;9:676-682.

How to cite this article: Day CR, Hanly JJ, Ren A, Martin A. Sub-micrometer insights into the cytoskeletal dynamics and ultrastructural diversity of butterfly wing scales. *Developmental Dynamics*. 2019;248:657–670. https://doi.org/10.1002/dvdy.63